# Infiltration in Unsaturated Layered Fluvial Deposits at Rio Bravo: Macroscopic Anisotropy and Heterogeneous Transport

R. J. Glass, J. R. Brainard,* and T.-C. Jim Yeh

## ABSTRACT

**An infiltration and dye transport experiment was conducted to visualize flow and transport processes in a heterogeneous, layered, sandy-gravelly fluvial deposit adjacent to Rio Bravo Boulevard in Albuquerque, NM. Water containing red dye followed by blue-green dye was ponded in a small horizontal zone (about 0.5 by 0.5 m) above a vertical outcrop (about 4 by 2.5 m). The red dye lagged behind the wetting front due to slight adsorption, thus allowing both the wetting front and dye fronts to be observed in time at the outcrop face. After infiltration, vertical slices were excavated to the midpoint of the infiltrometer, exposing the wetting front and dye distribution in a quasi three-dimensional manner. At small scale, wetting front advancement was influenced by the multitude of local capillary barriers within the deposit. However, at the scale of the experiment, the wetting front appeared smooth with significant lateral spreading, twice that in the vertical, indicating a strong anisotropy due to the pronounced horizontal layering. The dye fronts exhibited appreciably more irregularity than the wetting front, as well as the influence of preferential flow features (a fracture) that moved the dye directly to the front, bypassing the fresh water between. To illustrate the ability of equivalent homogeneous media models to capture the behavior of the wetting front, we performed numerical simulations using equivalent homogeneous media with isotropic, anisotropic, and moisture-dependent anisotropic properties. Those containing anisotropy matched the experimental data best.**

In the past two decades, numerous studies have investigated the effects of flow and solute transport in variably saturated media. Theoretical work (e.g., Yeh and Gelhar, 1983; Mualem, 1984; Yeh et al., 1985a, 1985b, 1985c; Mantoglou and Gelhar, 1987; Green and Freyberg, 1995), numerical simulations (e.g., Yeh, 1989; Desbarats, 1998; Wildenschild and Jensen, 1999b; Bagtzoglou et al., 1994; Polmann et al., 1991; Ababou, 1988; Ababou et al., 1991; Khaleel et al., 2002), and experimental studies (e.g., Stephens and Heerman, 1988; Yeh and Harvey, 1990; McCord et al., 1991; Wildenschild and Jensen, 1999a) indicate that if stratified sediments are regarded as an equivalent homogeneous medium, the effective hydraulic conductivity (**K**) tensor for the equivalent medium can exhibit moisture- or tension-dependent anisotropy. That is, the anisotropy (ratio of **K** parallel to bedding to **K** perpendicular to bedding) increases with decreasing saturation (increasing tension). For solute transport, several studies (e.g., Mantoglou and Gelhar, 1985; Polmann, 1990; Russo, 1993; Harter and Yeh, 1996; Roth and Hammel, 1996; Birkholzer and Tsang, 1997) suggest that in unsaturated media, the macrodispersivity for the equivalent homogeneous medium, which is in general anisotropic, increases with a decrease in saturation. The results of all these studies suggest that accounting for anisotropy in the modeling of flow and transport within the vadose zone may be important. However, most of these studies have focused on a theoretical analysis of the flow and transport behavior in synthetic media where the media is considered simply composed of distinct individual macroscopic layers within a stratigraphic sequence.

Natural sedimentary sequences can be quite complex with layers that are highly variable in thickness and lateral extent. Often, macroscopic layers, or units, are identified though sedimentological mapping, with differences between the units reflecting changes in the local depositional environment, origin of the sediments, stream dynamics, or subsequent superposition of pedogenic processes. As an example, refer to Fig. 1a, where a sequence of macrounits have been identified using sedimentological mapping methods within an outcrop of fluvial origin at the Rio Bravo site in Albuquerque, NM. A close inspection of individual macroscopic units within the stratigraphic sequence reveals each unit to be composed of a hierarchy of many subunit layers, as can best be seen in Fig. 1b. Such subunit layers are typical of deposits where eolian and fluvial processes have deposited the initial sequence of strata. At small scale, the bedding is composed of alternating fine and coarse layers obviously truncated by local erosion and redeposition of sediments resulting in the superimposition of a variety of longer length scales that increase the variability within the macrounit. The now classic work of R.A. Bagnold spanning from the 1940s to the 1970s (e.g., Bagnold, 1941, 1973) has elucidated much of the physics of such sedimentological processes and the deposits they create.

During the past few decades, numerous field infiltration and tracer experiments (e.g., Wierenga et al., 1986; Sisson and Lu, 1984; Gee and Ward, 2001; Brainard, 1997; Brainard et al., 2004a) have been conducted to study infiltration and solute transport processes in the heterogeneous vadose zone. Monitoring of the processes in these field experiments has mainly relied on measurements of capillary pressure, moisture content, and tracer concentration, using a limited number of tensiometers, neutron access tubes, and suction lysimeters over a large area. As a consequence, these sparse measurements depict moisture and solute distributions only at low resolution and provide temporal changes of the processes only at the measurement locations and not beyond. Recent advanced geophysical surveys (e.g., cross-borehole ground penetrating radar and cross-borehole electric resistivity tomography) are allowing the imaging of these distribu-

R.J. Glass and J.R. Brainard, Flow Visualization and Processes Laboratory, Sandia National Laboratories, Albuquerque, NM; T.-C. Jim Yeh, Department of Hydrology and Water Resources, The University of Arizona, Tucson, AZ. Received 29 Dec. 2003. Original Research Paper. *Corresponding author (jrbrain@sandia.gov).

Published in Vadose Zone Journal 4:22–31 (2005).

677 S. Segoe Rd., Madison, WI 53711 USA

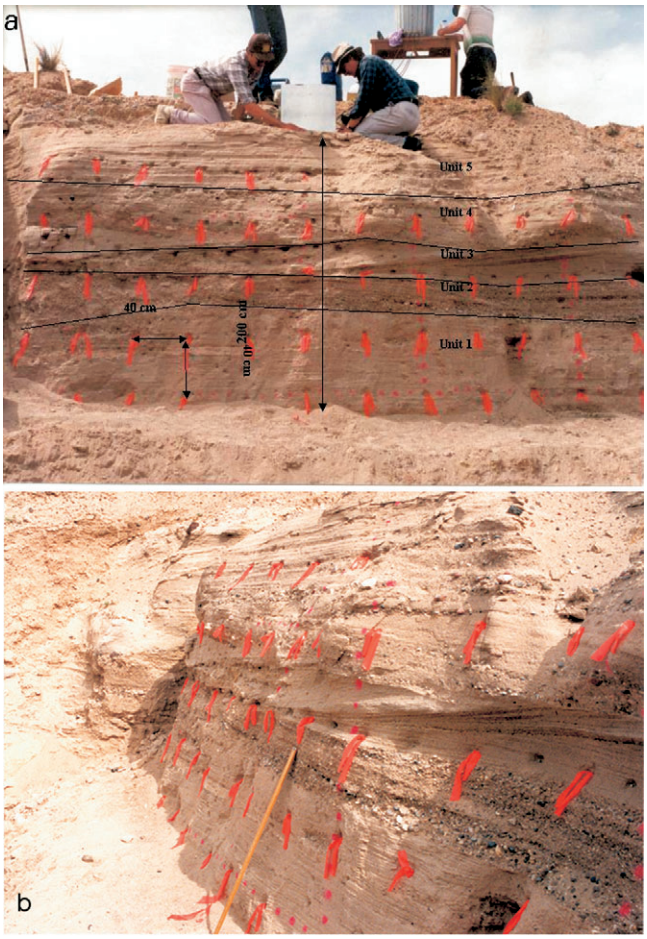


**Fig. 1. Layered fluvial outcrop at Rio Bravo. (a) View of outcrop taken during the final stages of infiltrometer installation and showing the contact locations of the five mapped units (see Table 1 for geologic description). The orange flags provided a 40 by 40 cm reference grid. (b) Oblique view of outcrop showing the outcrop profile. The infiltrometer is installed right of center just beyond the edge of the photograph. Note, these photographs should be seen in color and are best viewed on a computer screen where one can "zoom in" to see increasing detail.**

tions in multidimensions. Spatial resolution of these geophysical measurements, however, is limited, and their ability to accurately detect moisture content and solute concentration remains to be fully assessed (e.g., Alumbaugh et al., 2002; Yeh et al., 2002; Binley et al., 2001).

Here we present the results of a simple but unique field experiment designed to visualize processes occurring during water infiltration in a heterogeneous fluvial deposit with significant layering. We compare these results with illustrative numerical simulations based on the equivalent homogeneous medium concept. We infiltrated water containing slightly adsorbing dye tracers immediately above the vertical outcrop in the sandy-gravelly, fluvial deposit at Rio Bravo shown in Fig. 1. This design allowed documentation of the spatial and temporal evolution of both the wetting and lagging dye fronts on the face of the outcrop as infiltration progressed. Afterwards, we excavated the outcrop in vertical slices back from the face to visualize the dye and wetting front structure within the deposit. We provide images depicting the spatial evolution of the infiltrated dyes and water at both the outcrop and microlayering scales. We also discuss effects of multiscale heterogeneity on the movement of the dyes and water. Finally, we present results from qualitative simulations of the water infiltration process at the field site using equivalent homogeneous media for three cases: isotropic, constant anisotropic, and moisture-dependent anisotropic. Results of the simulation are discussed, and we emphasize the importance of including unsaturated hydraulic conductivity anisotropy in simulating water movement at the Rio Bravo field site.

## MATERIALS AND METHODS

Dye infiltration experiments have been used as a method to visualize vadose zone flow and transport processes during water infiltration in soils (e.g., Ghodrati and Jury, 1990; Flury et al., 1994) and in a variety of geologic deposits, including arid playa (Wierenga et al., 1986), sandy glacial outwash (Kung, 1990), glacial till (Roepke et al., 1995), sandy beach (Glass et al., 1988), a sand dune (McCord et al., 1991), and fractured volcanic tuff (Glass et al., 2002; Nicholl and Glass, 2002). In all of these field studies, the patterns of dye within the formation were obtained through site excavation by detailed mapping at the end of dye infiltration (i.e., one snapshot). In the experiment presented here, we wanted to capture a view of the evolving wetted zone and dye tracer structure as infiltration progressed, as well as at the end of infiltration. To do this we designed our experiment to infiltrate at the top of the vertical outcrop shown in Fig. 1 so we could obtain a continuous record of the spatial and temporal evolution at the face of the vertical outcrop. At the end of the experiment we excavated the site in a series of vertical cuts back into the outcrop. Because the dyes we used adsorbed slightly to the sediments, we were able to visualize both the wetting front and the fronts of the lagging dye tracers. A complete photographic record of our experiment can be found in Brainard and Glass (2004). We note that the photographs presented here must be seen in color and are best viewed on a computer screen where one can "zoom in" to see increasing detail.

### Site Description

The experimental site was located about 161 m (0.1 mile) east of I-25 on the south side of Rio Bravo Boulevard in Albuquerque, NM, where a road-cut provided a 2.5-m-high vertical exposure of ancestral Rio Grande layered sand and gravel (Fig. 2). These fluvial sediments were mapped into five macrounits having similar texture and structures and bounded by erosional contacts (see Table 1). They are predominantly weakly cemented and non- to slightly friable, except for the upper unit (Unit 5), which has moderately strong cementation and, as such, formed a resilient cap on the outcrop. Starting at the bottom, Unit 1 is a fine to coarse-grained sandstone and is bounded above by a pebble–granule conglomerate (Unit 2). The coarser grains in Unit 2 are supported by a matrix of medium to coarse sand. Unit 3 is a medium to coarse–grained sandstone capped by the fine to medium–grained sands of Units 4 and 5. The lack of pebble gravel interbeds in Units 5 and 3 distinguishes these units from Unit 4. In addition, within each unit, well-developed laminations and cross-bedding with thickness on the order of millimeters to centimeters were observed, reflecting both flowing fluid deposition and sequential fluvial deposition processes. A complete description of each of these units is presented in Table 1.

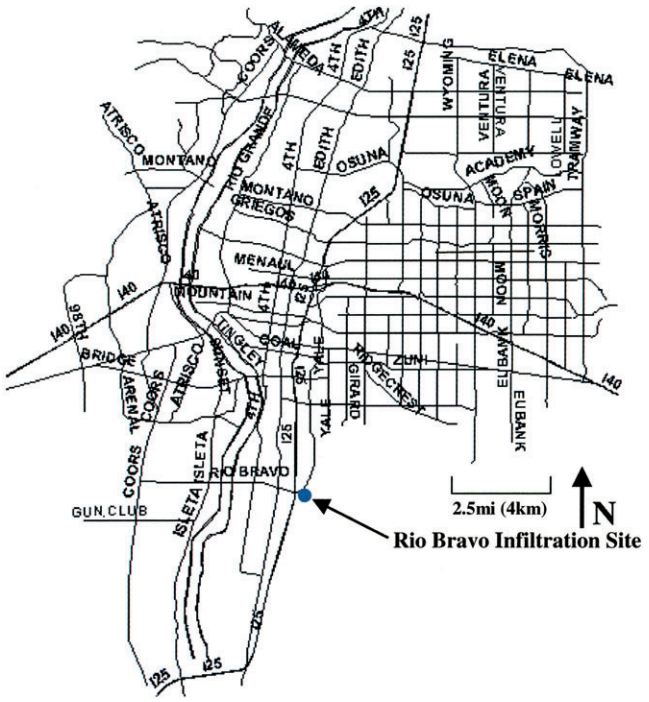


**Fig. 2. Location map of the Rio Bravo Site, located in southern Albuquerque, NM on the eastern escarpment of the "inner valley" resulting from the incision of the Rio Grande. The site is located on fluvial deposits within the Neogene/Quaternary Santa Fe Group, which comprise the principal fill of the Albuquerque Basin, one of the largest of a series of eastward stepping, en-echelon structural basins of the Rio Grande Rift (Kelley, 1977; Hawley, 1978).**

Because we did not wish to disturb the deposit before our visualization experiment, initial moisture content was not characterized. However, ambient moisture contents in similar deposits have been measured to be in the range of 3 to 8% (Brainard et al., 2004a).

### Site Preparation and Experimental Procedure

The top of the outcrop was excavated to provide a horizontal infiltration surface within Unit 5. A square infiltrometer (46 by 46 cm) was installed into this layer and equipped with float valves to provide a constant ponding depth of 1 to 2 cm. A supply tank (≈140 L) was used to mix the dye and feed the solution to the infiltrometer. Food coloring (Warner Jenkins Red Dye #3, Blue #1 and Green #3) was mixed with water at a concentration of approximately 1 g $L^{-1}$. At these concentrations, qualitative tests confirmed that the dyes adsorbed slightly to the sands and would lag behind the water. Infiltration was initiated 9 May 1992, with red-dyed water supplied for the first 20 h (370 L) followed by a mix of green and blue–dyed water lasting an additional 27 h (549 L). During this time, infiltration rate was recorded by measuring the levels in the supply tank. Cameras located directly in front of the outcrop recorded the progression of the wetting front and development of the dye plume. Photographs were taken at regular intervals during daylight hours. A 40-cm square grid marked on the face provided scale. Once infiltration was stopped, the outcrop was excavated in a series of vertical slices at 70, 60, 50, 43, 37, and 0 cm from the center of the infiltrometer to expose the internal structure of the dye plume. Each excavated face was photographed. Because the outcrop faced north, evaporation from the surface of the outcrop was minimized under ambient conditions. At night when photographs were not taken, the face of the outcrop was draped with a plastic tarp to further reduce evaporative losses.

## RESULTS

The observed infiltration rates followed the behavior of the standard infiltration equations and models (e.g., Kostiakov, 1932; Horton, 1933, 1939; Green and Amp, 1911; Philip, 1969) where the initial infiltration rate drops to a constant rate with time. Initially the infiltration rate was near 0.23 m $h^{-1}$ and dropped to near 0.085 m $h^{-1}$ by 7 h; thereafter it approached about 0.075 m $h^{-1}$ (Fig. 3). The slight variations in the rate after 7 h can be explained primarily by the influence of temperature variation during the test on the viscosity of the infiltrating water. On the first day, the ambient maximum temperature was 23°C. During the following night and into the next day, temperature dropped to a minimum of 21°C at the point where infiltration rate had reached its mini-

**Table 1. Geologic description of units, listed from the bottom of the outcrop to the top.**

**Unit 1: Fine to coarse, weakly cemented, nonfriable sandstone.**
- **Horizontal to subhorizontal carbonate indurated thin laminae**
- **Strata are mostly parallel with some low-angle cross-cutting relationships**
- **Carbonate cement is most abundant in the finer grained fractions near the top of the each stratum**
- **Sorted to poorly sorted fine sand at base and poorly sorted coarse sand and granules near the top**
- **Fining-upward sequences are present in the upper part of the unit**
- **Local zones of soft sediment deformation present along the left edges of the outcrop as viewed in Fig. 1**
- **Upper contact is located at the sharp textural transition to the Unit 2 conglomerate**

**Unit 2: Pebble–granule weakly cemented, slightly friable conglomerate with pebbles and granules, in a matrix of medium to coarse sand.**
- **Strata are laminae scale, planer and parallel with low-angle cross-cutting relationships; some local tangential cross laminae are also present**
- **Upper contact is located at the sharp textural transition to the Unit 3 sandstone**

**Unit 3: Fine to medium–grained weakly cemented, slightly friable sandstone**
- **Thinly laminated to laminated with local pebble and granule lags**
- **Strata are parallel and planer with abundant low-angle tangential cross stratification**
- **Coarse to very coarse sand with granules occurs locally, and pebble lags cap some erosional surfaces on the left side of the outcrop**
- **Carbonate cement concentrated at tops of strata**
- **Upper contact is located at the sharp textural transition to Unit 4**

**Unit 4: Fine to medium–grained weakly cemented, slightly friable sandstone**
- **Thin to very thin planer laminae with local interbeds of pebble–granule conglomerate**
- **Laminae are mostly parallel but locally display low-angle cross-cutting relationships**
- **Cobble-sized rip-up clasts of sandstone and mudstone occur near the base**
- **Upper contact is picked at the top of a bedding plane, above which pebble–granule interbeds are not present**

**Unit 5: Medium to fine–grained moderately cemented sandstone**
- **Planar and parallel thin laminae and thin beds with occasional lag pebbles**
- **Low-angle cross-cutting relationships are rare**
- **Upper contact is not exposed in the outcrop**

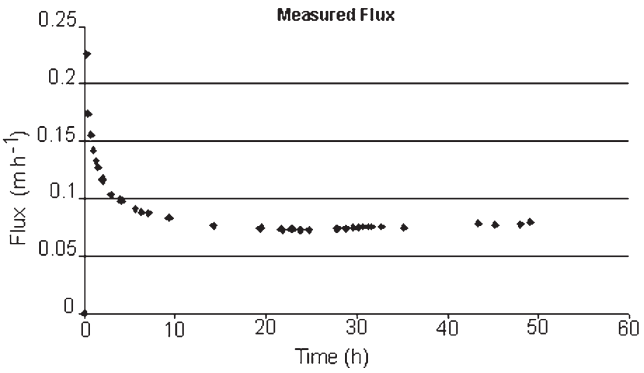


**Fig. 3. Experimental infiltration rate plotted for the approximately 47-h infiltration experiment.**

mum, after which it began to rise. On the last day of the experiment, the temperature had increased to 26°C when the infiltration was 0.079 m $h^{-1}$ and slowly rising.

The visual contrast between wet and dry regions, the red dye tracer, and the subsequent darker dyes resulted in vivid photographs showing the development of the wetting front and dye plumes with time. As an example, Fig. 4 shows the photograph taken at approximately 48 h. The outermost zone of higher moisture content behind the wetting front was primarily free of red dye because of its slight adsorption to the sand. Locations of the three fronts in time are shown in composite drawings obtained by digitizing the locations of the fronts from the photographs taken throughout the infiltration experiment (Fig. 5a–5c; a complete set of photographs can be found in Brainard and Glass (2004). Photographs of the excavated faces provided a quasi-three-dimensional view of the internal structure of the plume (Fig. 6a–6f).

Despite the heterogeneous nature of the deposits, the overall wetting front remained relatively smooth and symmetrical throughout infiltration. Across all photographs, we see enhanced lateral spreading relative to vertical penetration (i.e., lateral spreading ≈ twice vertical spreading) beginning early in the experiment and continuing throughout its duration. The multitude of small, sequential, capillary barriers within and across each mapped unit caused only local irregularity in wetting and integrated to create a smooth large-scale anisotropic structure. An example of this local action is shown in the photographs of Fig. 7a and 7b. There, at 30 h into infiltration, the local flow at the lower edge of the wetted bulb was blocked by a stronger than average capillary barrier (coarser top of the ≈20-cm-thick cross-bedded Unit 3 noted in Fig. 7a). Subsequent breakthrough followed the irregular cross bedding directly below. While the bottom of the advancing front is held back by the sequential action of a multitude of these fine–coarse capillary barriers, this same sequence allows effective horizontal movement with only a sight irregularity at the edges (Fig. 7b).

In contrast to the macroscopically smooth wetting fronts, dye fronts exhibited much greater irregularity. While we can see this in the sequence of photographs taken as infiltration progressed, those of the excavation at the end of the test show this more vividly (Fig. 6a–6f). These photographs show that both the red and blue-green dye fronts contained "streamers" that radiated both laterally and downward from the center of the plume. Some of the streamers persisted with depth into the formation, as evidenced by similarity between shape and location from one photograph to the next. Only one of these streamers could be associated with an obvious

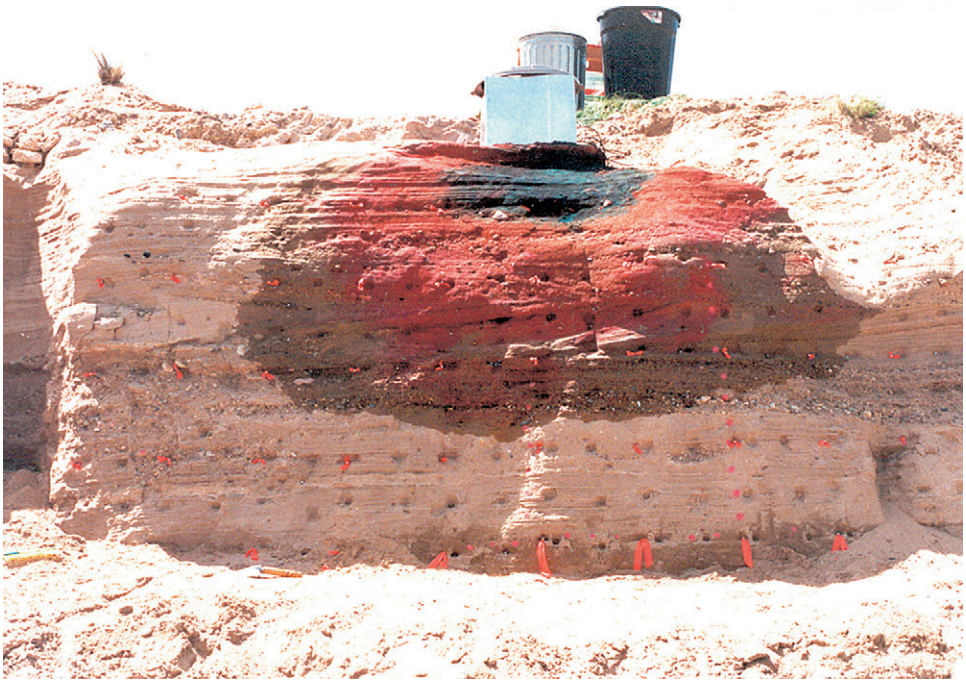

**Fig. 4. Photo of plume development at about 48 h. Three zones are visible: an outer clear water zone, a middle red dye zone, and an inner blue-green zone. Note that this photograph should be seen in color and is best viewed on a computer screen where one can "zoom in" to see increasing detail.**

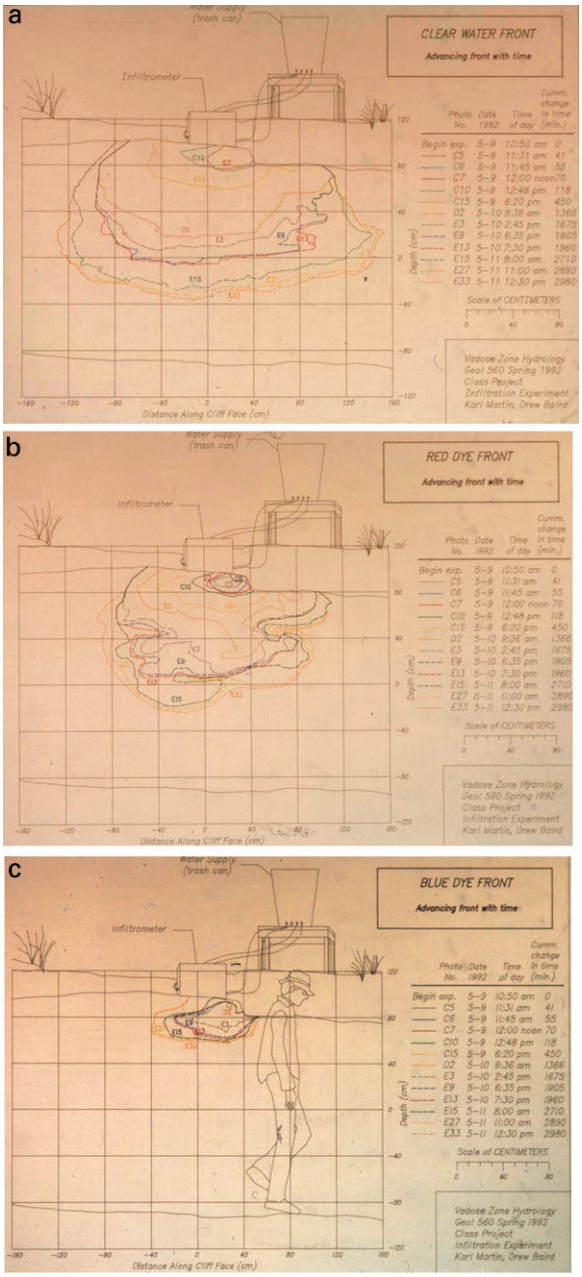


**Fig. 5. Composite drawings of water, red and blue fronts, depicting the location of the three fronts in time for (a) water, (b) red dye, and (3) blue dye.**

preferential flow feature. A near vertical fracture that extended into the face outcrop and ran up toward the left hand corner of the infiltrometer (but did not penetrate into the top unit) could be seen to transport dye significantly ahead of the rest of the dye front (Fig. 8). While this fracture seemed to have very little influence on the advance of wetting, Fig. 8 shows it to provide red dye (and thus water) directly to the wetting front. Tracing this fracture back into the outcrop in the excavated slices of Fig. 6a through 6f shows its influence on the blue-green dye front to persist back to just before the midpoint of the infiltrometer (Fig. 6e).

## Illustrative Simulations with Equivalent Homogeneous Media

Even in the midst of significant visual heterogeneity (Fig. 1), the wetting front at Rio Bravo formed a symmetric, horizontally anisotropic plume (i.e., lateral spreading ≈ twice vertical spreading). This behavior suggests the possible applicability of equivalent homogeneous media concepts for modeling water infiltration in such deposits. As an illustration of this applicability, we conducted several simple numerical simulations. A two-dimensional cross section ($x$–$z$ plane, where $x$ is the horizontal axis and $z$ is the vertical) of the field site was created as a simulation domain, 3.2 m in the horizontal direction and 1.8 m in the vertical, reflecting the actual size of the outcrop. This domain was discretized into 32 × 18 elements of 0.1 by 0.1 m each. The bottom of the domain was assumed to be under a unit gradient condition; the left- and right-hand sides and top of the domain, except the center zone corresponding to the infiltrometer, were assumed to be no-flow boundaries. A ponded constant head boundary was assumed for the center portion of the top boundary. The initial pressure distribution was assumed uniform at −10 m of water (corresponding to ≈4% initial moisture content for properties as presented below).

The unsaturated hydraulic conductivity and moisture release curves for the homogeneous medium were taken to follow the Mualem–van Genuchten model (van Genuchten, 1980):

$$\theta(h) = (\theta_s - \theta_r)[1 + (\alpha|h|)^n]^{-m} + \theta_r \quad [1a]$$

$$K(h) = K_s\{1 - (\alpha|h|)^{(n-1)}[1 + (\alpha|h|)^n]^{-m}\}^2/[1 + (\alpha|h|)^n]^{(m/2)} \quad [1b]$$

where $h$ is the capillary pressure head, $K_s$ is the saturated hydraulic conductivity, and $\alpha$ and $n$ are shape factors, with $m = 1 - 1/n$. The saturated moisture content is $\theta_s$, and residual moisture content is $\theta_r$. Base values for all the parameters were found to allow a "by eye" fit of the macroscopic wetting front behavior (our effective measure). Note that further adjustment of these parameters for our two-dimensional simulations to better fit a three-dimensional experiment is of limited value.

To illustrate the importance of anisotropy we considered three cases: isotropic (Case 1), constant anisotropic (Case 2), and moisture-dependent anisotropic (Case 3). For Case 1 all parameters of Eq. [1a] and [1b] were taken to be the same in the $x$ and $z$ directions. For Case 2, the saturated hydraulic conductivity in the $x$ direction was set to be three times that in the $z$ direction, while the rest of the parameters were taken to be directionally independent. Finally, for Case 3, in addition to the directional preference in $K_s$, the parameter $\alpha$ in the hydraulic conductivity–pressure head relation (Eq. [1b]) was taken to be directionally dependent. Note that the deviations from base parameter values in Case 1 chosen to reflect anisotropy, were chosen for illustrative purposes; the values of all parameters for each of the three cases are listed in Table 2. With these parameter values and the omission of hysteresis, a finite element model for vari-

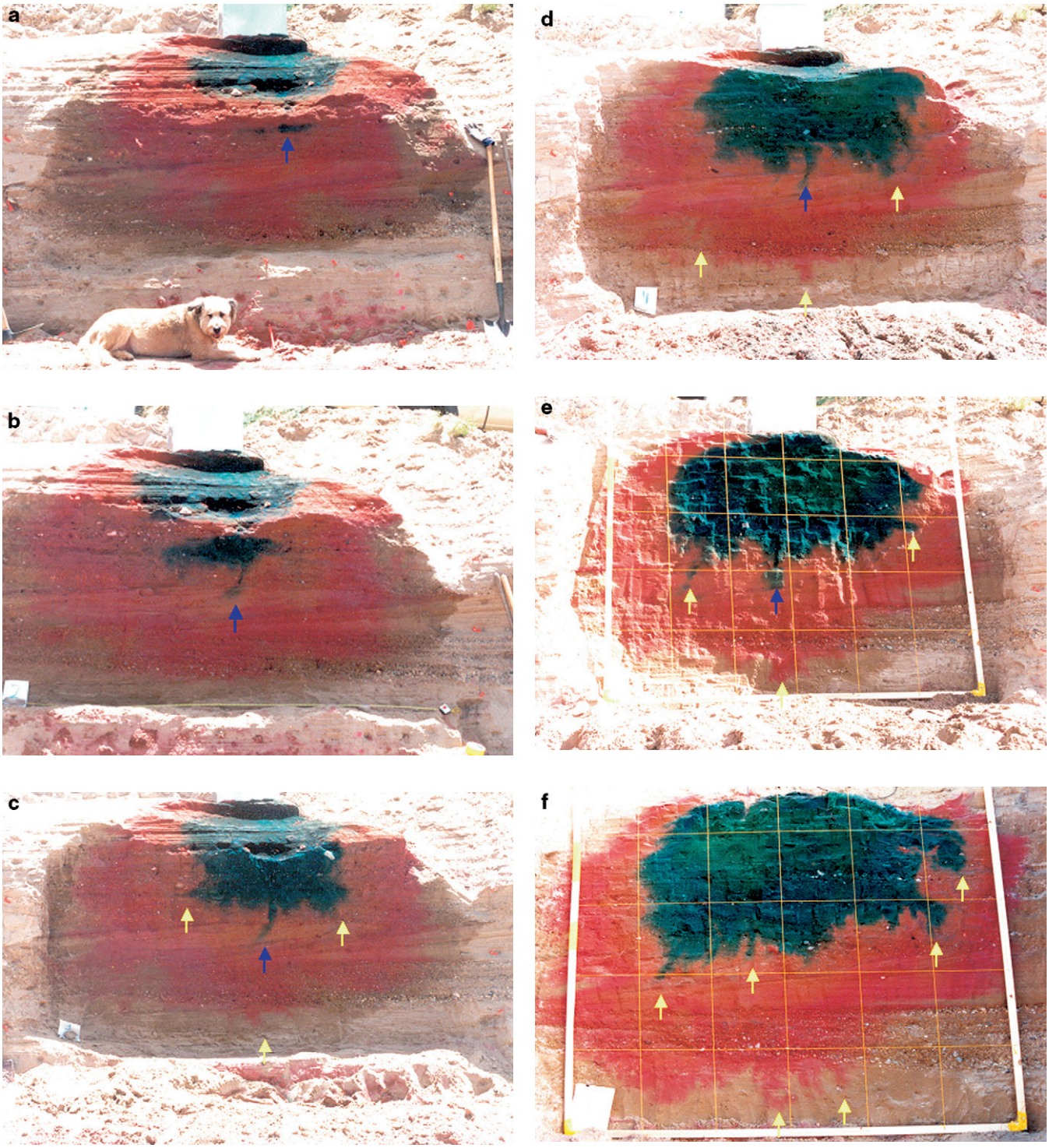


**Fig. 6. Series of photographs taken after excavating slices from the outcrop face shown in Fig. 1 and Fig. 4. The excavated faces are exposed at 70, 60, 50, 43, 37, and 0 cm from the center of the infiltrometer. Notice the red and blue-green streamers radiating from the center of the plume, some of which have been identified with yellow arrows. A blue arrow designates the location of a fracture within the deposit that extended back from the outcrop face and influenced dye transport (see Fig. 8 as well). Note, these photographs should be seen in color and are best viewed on a computer screen where one can "zoom in" to see increasing detail.**

ably saturated flow and transport (Yeh et al., 1993, VSAFT2, which is available at www.hwr.arizona.edu/yeh [verified 13 Oct. 2004]) was employed to simulate the infiltration event.

Figures 9, 10, and 11 show the simulated moisture distribution at about 18 h after the beginning of infiltration in the homogeneous medium for Cases 1, 2, and 3, respectively. The homogeneous and isotropic medium (Case 1) produced predominantly vertical migration of the infiltrated moisture. The medium with either constant

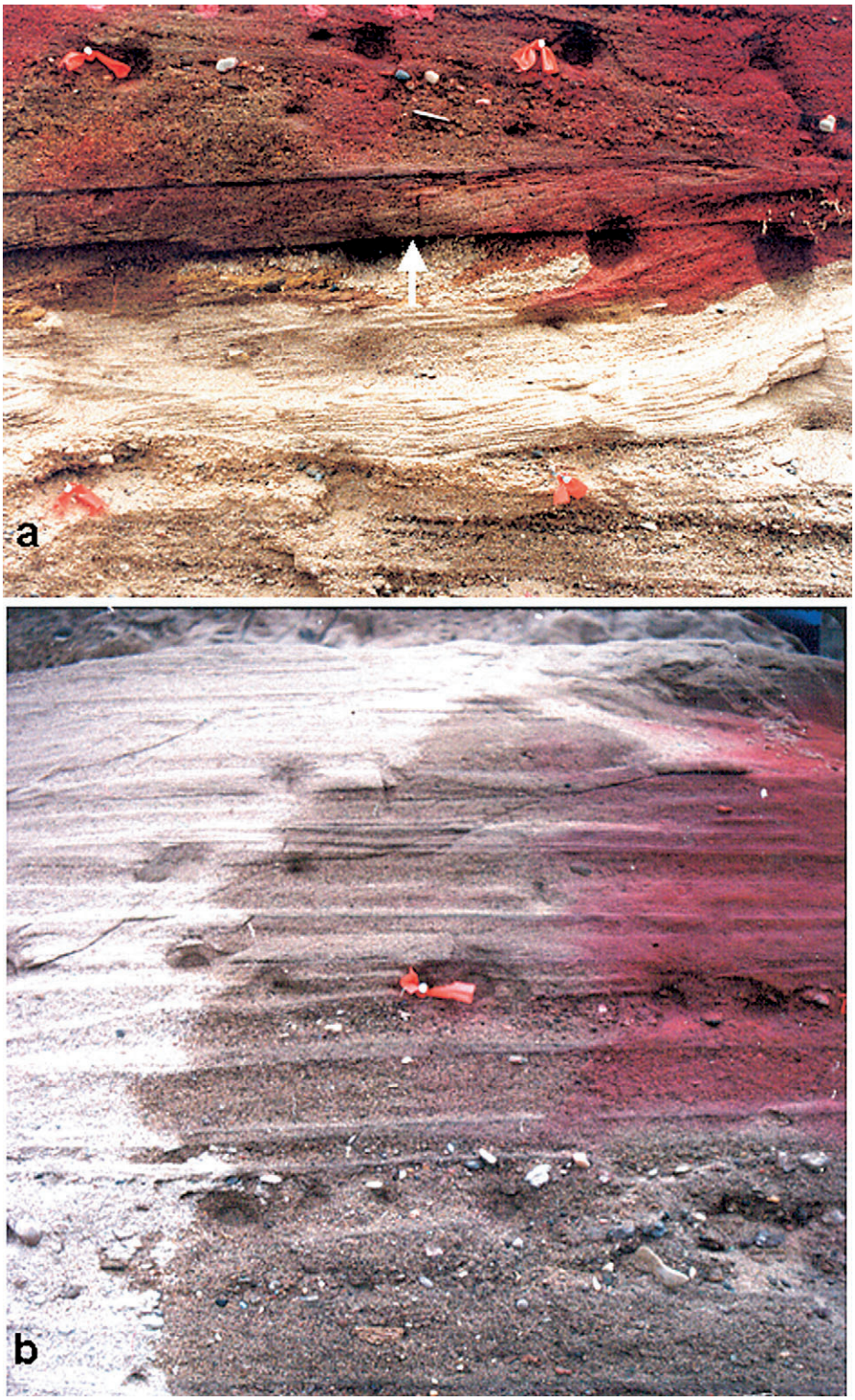


**Fig. 7. Example influence of layering. Close-up photographs of the (a) bottom and (b) side of the plume at about 30 h. At the bottom, water appears to be preferentially flowing parallel to small-scale cross bedding after breaking through a stronger horizontal capillary barrier at the top of unit 3 (white arrow). At the side, these sequential capillary barriers allow effective horizontal flow. Note, these photographs should be seen in color and are best viewed on a computer screen where one can "zoom in" to see increasing detail.**

anisotropy or moisture-dependent anisotropy (Cases 2 or 3) resulted in greater horizontal spreading of the infiltrated water than the medium with isotropy. Comparing the resultant moisture distributions of Cases 2 and 3 with the observed wetting front (Fig. 5a), both are qualitatively similar to the experiment. However, it appears that the medium with the moisture-dependent anisotropy yields a slightly better match with a blunter moisture distribution at the bottom of the plume than is represented with the constant anisotropy medium.

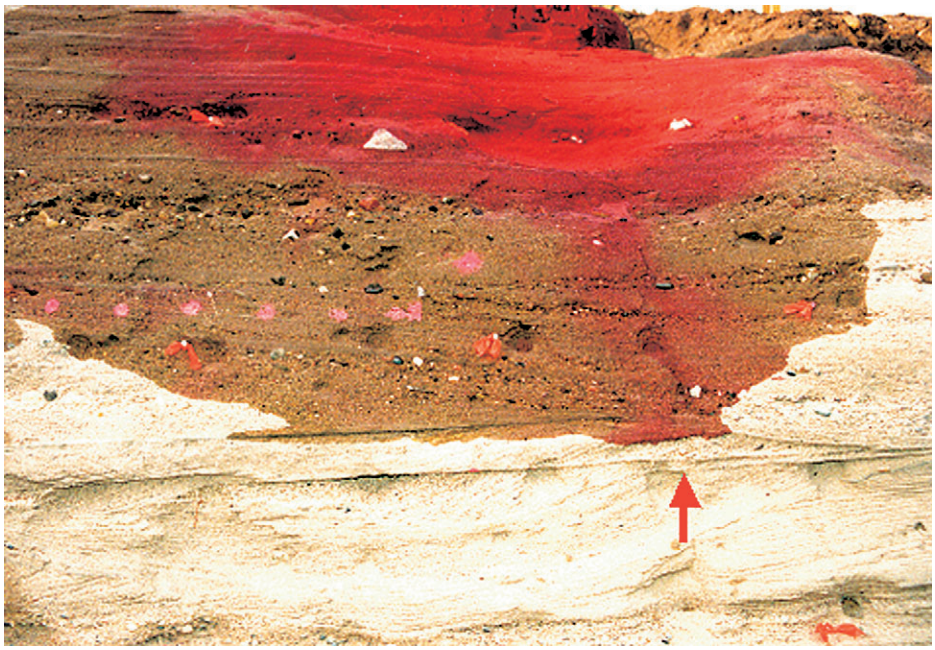

**Fig. 8. View of the plume showing a red streamer intruding along the fracture to the clear water front (red arrow). This photo of the unexcavated face was taken about 30 h after start of infiltration. Note, this photograph should be seen in color and is best viewed on a computer screen where one can "zoom in" to see increasing detail.**

## CONCLUSIONS

The field experiment at the Rio Bravo site provided an excellent illustration of the spatial and temporal evolution of infiltrating water in a layered fluvial deposit. The deposit encompassed five mapped units, each of which contained a multitude of smaller-scale layers that ranged in thickness from several centimeters to millimeters and had horizontal length scales ranging from several centimeters up to the width of our experiment and beyond. Yet, in this complex heterogeneous structure, a simple regular plume emerged. Small-scale irregularities at the wetting front averaged to yield a macroscopically smooth wetting front with significant anisotropy (i.e., lateral spreading ≈ twice vertical spreading). We found that replacing the heterogeneous deposit with a simple equivalent anisotropic homogeneous media easily reproduced such a structure. This observation appears to support the results of theoretical and laboratory experiments, reviewed in our introduction, that suggest such anisotropy to arise in layered unsaturated deposits.

While a number of infiltration experiments have been conducted in the heterogeneous vadose zone (e.g., Wierenga et al., 1986; Sisson and Lu, 1984; Gee and Ward, 2001; Brainard, 1997; Brainard et al., 2004a), none have shown such smooth, nearly symmetrical, and ellipsoidal moisture fronts as the Rio Bravo experiment. This difference may be because the geological settings of these other experiments contained more significant large-scale variability in hydraulic properties, resulting in the formation of experiment-scale, nonsymmetrical, preferential flow and solute transport. At Rio Bravo, our results suggest that variability in properties and structure between the different mapped units was not significant at the scale of the experiment, thus resulting in a symmetrical, ellipsoidal wetting front. Indeed, while one may designate units within the deposit to be separate sedimentologically, from a hydrological point of view, we seem to be able to describe the deposit as single hydrostratigraphic unit with its multitude of layers represented by an equivalent homogeneous medium. In this sense, the Rio Bravo site, at least at the scale of our experiment, is ideally suited for the application of equivalent homogeneous media concepts that incorporate anisotropy due to the homogenization of layering.

Results at Rio Bravo also demonstrate that behind the wetting front dye transport appears more heterogeneous and includes preferential movement directly to the front in the context of crosscutting features (e.g., fractures). Because capillary pressure variability naturally decreases behind a wetting front, flow and thus advective transport behind the wetting front will be increasingly controlled by the differences in the hydraulic conductivity within the zone. In addition, movement of the dye will also be influenced if its adsorption varies in space.

**Table 2. Properties used in illustrative numerical simulations.**

| | Parameters for unsaturated hydraulic conductivity function | | | | | | Parameters for moisture release curve | | | |
|---|---|---|---|---|---|---|---|---|---|---|
| | $K_{s-x}$ | $K_{s-z}$ | $\alpha_x$ | $\alpha_z$ | $n_x$ | $n_z$ | $\alpha$ | $n$ | $\theta_s$ | $\theta_r$ |
| | | | cm $s^{-1}$ | | | | 1 $cm^{-1}$ | | | |
| Isotropic | 0.001 | 0.001 | 0.0335 | 0.0335 | 3.0 | 3.0 | 0.0335 | 3.0 | 0.368 | 0.102 |
| Constant anisotropy | 0.003 | 0.001 | 0.0335 | 0.0335 | 3.0 | 3.0 | 0.0335 | 3.0 | 0.368 | 0.102 |
| Moisture-dependent anisotropy | 0.003 | 0.001 | 0.0335 | 0.0435 | 3.0 | 3.0 | 0.0335 | 3.0 | 0.368 | 0.102 |

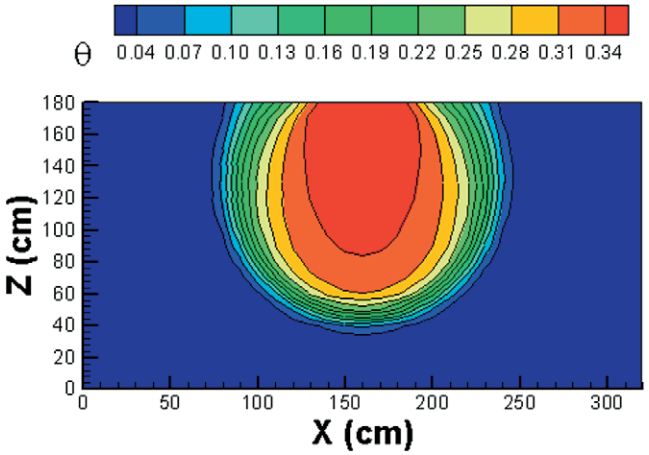


**Fig. 9. Homogeneous isotropic simulation: Simulated moisture distribution at about 18 h after infiltration in an equivalent homogeneous medium with isotropic unsaturated hydraulic conductivity.**

Regardless of whether variable flow (advection), variable adsorption, or some other process is responsible, the difference in structure between the wetting and dye fronts is interesting and encourages additional study in the future.

In conclusion, we emphasize that both the infiltration experiment at Rio Bravo and the numerical simulations presented here were designed as illustrative. Results show that the effect of layering is clearly significant in the natural fluvial deposit at Rio Bravo. Importantly, we found that for the advance of the wetting front, all the detailed small-scale behavior at the front averaged to produce a large-scale macroscopic symmetrical plume. Our numerical simulations show that representing the heterogeneous deposit with an equivalent homogeneous medium requires an effective, large-scale hydraulic conductivity anisotropy to reproduce the enhanced horizontal migration of water observed in the experiment. Such an anisotropic hydraulic conductivity function has been frequently ignored in the analysis of flow and solute transport in the vadose zone and would yield significant errors in deposits such as those at Rio Bravo. Although the necessity of anisotropy is clear, whether that

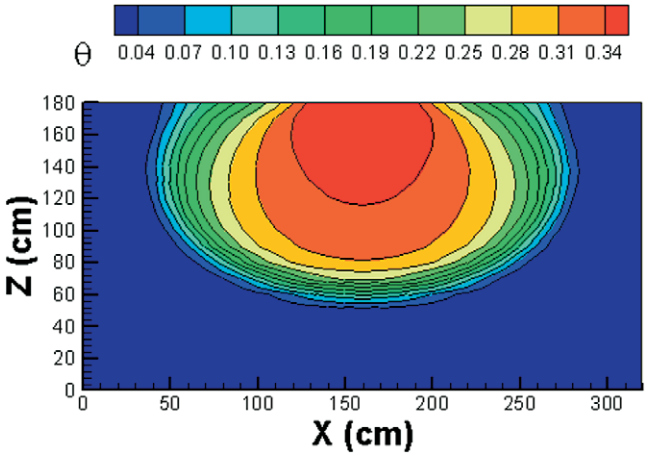


**Fig. 10. Homogeneous constant anisotropic simulation. Simulated moisture distribution at about 18 h after infiltration in an equivalent homogeneous medium with a constant unsaturated hydraulic conductivity anisotropy.**

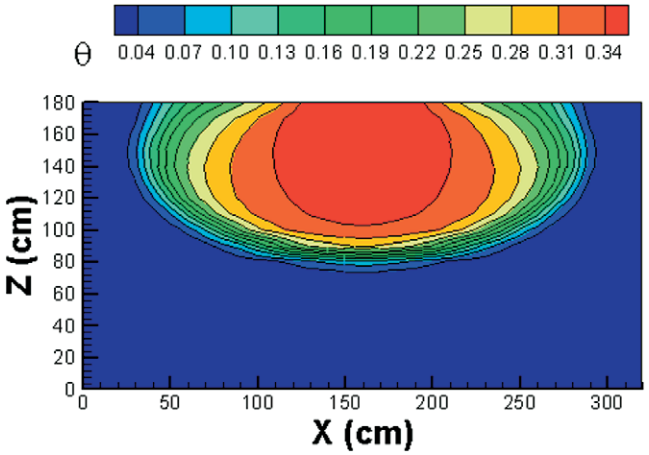


**Fig. 11. Homogeneous moisture-dependent anisotropic simulation. Simulated moisture distribution at about 18 h after infiltration in an equivalent homogeneous medium with a moisture-dependent unsaturated hydraulic conductivity anisotropy.**

anisotropy is moisture-dependent or constant remains to be fully considered. To investigate this and other issues further, additional large-scale infiltration experiments are required that include extensive site characterization as well as the application of accurate, quantitative, real-time monitoring of moisture content and pressure fields.

## ACKNOWLEDGMENTS

This experiment was conducted as part of a Vadose Zone class project taught by R.J. Glass at the University of New Mexico in 1992. Class participants included Karl Martin, Drew Baird, Jim Brainard, Bob Holt, Dan Garrett, and Rick Morris. Portions of this field experiment were reported in Martin et al. (1993) and Glass and Nicholl (1996), as well as at many national scientific meetings since 1992. We acknowledge funding from DOE's Environmental Management and Science Program under contract DE-AC04-94 AL85000 to Sandia National Laboratories for the analysis of the data and preparation of the manuscript. The numerical simulation work by the third author was funded by EPA STAR program R-827114-01-0 and NSF grant (EAR-0229717).

## REFERENCES

Ababou, R. 1988. Three-dimensional flow in random porous media. Ph.D. diss. Massachusetts Inst. of Technology, Cambridge, MA.

Ababou, R., A.C. Bagtzoglou, B. Sagar, and G. Wittmeyer. 1991. Stochastic analysis of flow and transport. p. Chapter 6 *In* W.C. Patrick (ed.) Report on Research Activities for Calendar Year 1990. Rep. NUREG/CR-5817. U.S. Nuclear Regulatory Commission, Washington, DC.

Alumbaugh, D., L. Paprocki, J.R. Brainard, R.J. Glass, and C. Rautman. 2002. Estimating initial moisture contents using cross-borehole ground penetrating radar: A study of accuracy and repeatability. Water Resour. Res. 38(12):1309. doi:10.1029/2001WR000754.

Bagnold, R.A. 1941. The physics of blown sand and desert dunes. Chapman and Hall, London.

Bagnold, R.A. 1973. The nature of saltation and of bed load transport in water. Proc. R. Soc. London, Ser. A 332:473–504.

Bagtzoglou, A.C., S. Mohanty, A. Nedungadi, T.-C.J. Yeh, and R. Ababou. 1994. Effective hydraulic property calculations for unsaturated fractured rock with semi-analytical and direct numerical techniques: Review and applications. CNWRA Rep. 94-007. Center for Nuclear Waste Regulatory Analyses, Southwest Research Institute, San Antonio, TX.

Binley, A, P. Winship, R. Middleton, M. Pokar, and J. West. 2001. High-resolution characterization of vadose zone dynamics using

cross-borehole radar. Water Resour. Res. 37(11). doi:10.1029/2000wr000089.
Birkholzer, J., and C.-F. Tsang. 1997. Solute channeling in unsaturated heterogeneous media. Water Resour. Res. 33:2221–2238.
Brainard, J.R. 1997. Vadose zone flow processes in heterogeneous alluvial fan deposits: Experimental design, data evaluations, and error analysis. M.S. thesis. Department of Earth and Planetary Sciences, University of New Mexico, Albuquerque.
Brainard, J.R., and R.J. Glass. 2004. The Rio Bravo infiltration and dye transport study: A photo essay. SAND Rep. Sandia Natl. Lab., Albuquerque, NM.
Brainard, J.R., R.J. Glass, D.L. Alumbaugh, L. Paprocki, D.J. La Brecque, X. Yang, T.-C.J. Yeh, K.E. Baker, and C.A. Rautman. 2004. The Sandia-Tech Vadose Zone Facility: Experimental design and data report of a constant flux infiltration experiment. SAND Report. Sandia Natl. Lab., Albuquerque, NM.
Desbarats, A.J. 1998. Scaling of constitutive relationships in unsaturated heterogeneous media. Water Resour. Res. 34:1427–1436.
Flury, M., H. Flühler, W.A. Jury, and J. Leuenberger. 1994. Susceptibility of soils to preferential flow of water: A field study. Water Resour. Res. 30:1945–1954.
Gee, G.W., and A.L. Ward. 2001. Vadose zone transport field study: Status report. PNNL-13679. Pacific Northwest Natl. Lab., Richland, WA.
Ghodrati, M., and W.A. Jury. 1990. A field study using dyes to characterize preferential flow of water. Soil Sci. Soc. Am. J. 54:1558–1563.
Glass, R.J., and M.J. Nicholl. 1996. Physics of gravity driven fingering of immiscible fluids within porous media: An overview of current understanding and selected complicating factors. Geoderma 70: 133–163.
Glass, R.J., M.J. Nicholl, A.L. Ramirez, and W.D. Daily. 2002. Liquid phase structure within an unsaturated fracture network beneath a surface infiltration event: Field experiment. Water Resour. Res. 38(10):1199. doi:10.1029/2000WR000167.
Glass, R.J., T.S. Steenhuis, and J-Y. Parlange. 1988. Wetting front instability as a rapid and far-reaching hydrologic process in the vadose zone. J. Contam. Hydrol. 3(2–4):207–226.
Green, W.H., and G.A. Amp. 1911. Studies in soil physics. I. The flow of air and water through soils. J. Agric. Sci. 4:1–24.
Green, T.R., and D.L. Freyberg. 1995. State-dependent anisotropy: Comparisons of quasi-analytical solutions with stochastic results for steady gravity drainage. Water Resour. Res. 31:2201–2212.
Harter, T., and T.-C.J. Yeh. 1996. Stochastic analysis of solute transport in heterogeneous, variably saturated soils. Water Resour. Res. 29:4139–4149.
Hawley, J.W. 1978. Guide book to the Rio Grande Rift in New Mexico and Colorado. Circular 163. New Mexico Bureau of Mines and Mineral Resources, Socorro.
Horton, R.E. 1933. The role of infiltration in the hydrologic cycle. Trans. AGU, 14th Ann. Mtg., p. 446–460.
Horton, R.E. 1939. Analysis of runoff-plot experiments with varying infiltration capacity. Trans. AGU, 20th Ann. Mtg., Part IV, p. 693–694.
Kelley, V.C. 1977. Geology of Albuquerque Basin, New Mexico. Memoir 33. New Mexico Bureau of Mines and Mineral Resources, Socorro.
Khaleel, R., T.-C. J. Yeh, and Z. Lu. 2002. Upscaled flow and transport properties for heterogeneous unsaturated media. Water Resour. Res. 38(5). doi:10.1029/2000WR000072.
Kostiakov, A.N. 1932. On the dynamics of the coefficient of water percolation in soils and the necessity of studying it from a dynamic view for the purpose of amelioration. Trans. 6th Congr. Int. Soc. Sci., Russian part A:17–21.
Kung, K.J.S. 1990. Preferential flow in a sandy vadose zone. 1. Field Observation. Geoderma 46(1–3):51–58.
Mantoglou, A., and L.W. Gelhar. 1985. Large-scale models of transient unsaturated flow and contaminant transport using stochastic methods. Ralph M. Parsons Laboratory Tech. Rep. 299. Massachusetts Institute of Technology, Cambridge, MA.
Mantoglou, A., and L.W. Gelhar. 1987. Stochastic modeling of large-scale transient unsaturated flow. Water Resour. Res. 23:37–46.
Martin, K.A., D.C. Baird, and R.J. Glass. 1993. Infiltration into thick unsaturated alluvial deposits: A preliminary study. p. 174–179. *In* Proc. of the 1993 National Conf. on Hydraulic Engineering and International Symposium on Engineering Hydrology, San Francisco, CA. 25–30 July 1993. ASCE, Reston, VA.
McCord, J.T., D.B. Stephens, and J.L. Wilson. 1991. Hysteresis and state-dependent anisotropy in modeling unsaturated hill slope hydrologic processes. Water Resour. Res. 27:1501–1518.
Mualem, Y. 1984. Anisotropy of unsaturated soils. Soil Sci. Soc. Am. J. 48:505–509.
Nicholl, M.J., and R.J. Glass. 2002. Field investigation of flow processes in an initially dry fracture network at Fran Ridge, Yucca Mountain, Nevada: A photo essay and data summary. SNL Paper SAND02-1369. Sandia Natl. Lab., Albuquerque, NM.
Philip, J.R. 1969. The theory of infiltration. Adv. Hydrosci. 5:215–296.
Polmann, D.J. 1990. Application of stochastic methods to transient flow and transport in heterogeneous unsaturated soils. Ph.D. diss. Massachusetts Inst. Technol., Cambridge, MA.
Polmann, D.J., D. Mclaughlin, S. Luis, L.W. Gelhar, and R. Ababou. 1991. Stochastic modeling of large-scale flow in heterogeneous unsaturated soils. Water Resour. Res. 27:1447–1458.
Roepke, C., R.J. Glass, J. Brainard, M. Mann, K. Kriel, R. Holt, and J. Schwing. 1995. Transport processes investigation: A necessary first step in site scale characterization plans. Proceedings of Waste Management 95, Tucson, AZ. 26 Feb.–7 Mar. 1995. Session 27, paper 20. SAND Rep. SAND95-0289C. Sandia Natl. Lab., Albuquerque, NM.
Roth, K., and K. Hammel. 1996. Transport of conservative chemical through an unsaturated two-dimensional Miller-similar medium with steady state flow. Water Resour. Res. 32:1653–1663.
Russo, D. 1993. Stochastic modeling of macrodispersion for solute transport in a heterogeneous unsaturated porous formation. Water Resour. Res. 29:383–397.
Sisson, J.B., and A.H. Lu. 1984. Field calibration of computer models for application to buried liquid discharges: A status report. RHO-ST-46P. Rockwell Hanford Operations, Richland, WA.
Stephens, D.B., and S. Heerman. 1988. Dependence of anisotropy on saturation in a stratified sand. Water Resour. Res. 24:770–778.
van Genuchten, M.Th. 1980. A closed-form equation for predicting the hydraulic conductivity of unsaturated soils. Soil Sci. Soc. Am. J. 44:892–898.
Wierenga, P.J., L.W. Gelhar, C.S. Simmons, G.W. Gee, and T.J. Nicholson. 1986. Validation of stochastic flow and transport models for unsaturated soils: A comprehensive field study. Rep. NUREG/CR466-22. U.S. Nuclear Regulatory Commission, Washington, DC.
Wildenschild, D., and K.H. Jensen. 1999a. Laboratory investigations of effective flow behavior in unsaturated heterogeneous sands. Water Resour. Res. 35:17–27.
Wildenschild, D., and K.H. Jensen. 1999b. Numerical modeling of observed effective flow behavior in unsaturated heterogeneous sands. Water Resour. Res. 35:29–42.
Yeh, T.-C.J. 1989. One-dimensional steady-state infiltration in heterogeneous soils. Water Resour. Res. 25:2149–2158.
Yeh, T.-C.J., and L.W. Gelhar. 1983. Unsaturated flow in heterogeneous soils. p. 71–79. *In* J.W. Mercer et al. (ed.) Role of the unsaturated zones in radioactive and hazardous waste disposal. Ann Arbor Science, Ann Arbor, MI.
Yeh, T.-C.J., L.W. Gelhar, and A.L. Gutjahr. 1985a. Stochastic analysis of unsaturated flow in heterogeneous soils: 1. Statistically isotropic media. Water Resour. Res. 21:447–456.
Yeh, T.-C.J., L.W. Gelhar, and A.L. Gutjahr. 1985b. Stochastic analysis of unsaturated flow in heterogeneous soils: 2. Statistically anisotropic media. Water Resour. Res. 21:457–464.
Yeh, T.-C.J., L.W. Gelhar, and A.L. Gutjahr. 1985c. Stochastic analysis of unsaturated flow in heterogeneous soils: 3. Observations and applications. Water Resour. Res. 21:465–471.
Yeh, T.-C.J., and D.J. Harvey. 1990. Effective unsaturated hydraulic conductivity of layered sands. Water Resour. Res. 26:1271–1279.
Yeh, T.-C.J., S. Liu, R.J. Glass, K. Baker, J.R. Brainard, D. Alumbaugh, and D. LaBrecque. 2002. A geostatistically based inverse model for electrical resistivity surveys and its applications to vadose zone hydrology. Water Resour. Res. 38:1278. doi:10.1029/2001WR001204.
Yeh, T.-C.J., R. Srivastava, A. Guzman, and T. Harter. 1993. A numerical model for two dimensional flow and chemical transport. Ground Water 31:634–644.